Supplementary Materials for

Farming and public goods production in *C. elegans* populations

Shashi Thutupalli, Sravanti Uppaluri, George W.A. Constable, Simon A. Levin, Howard A. Stone, Corina E. Tarnita, Clifford P. Brangwynne

correspondence to: S.T.: shashi@ncbs.res.in, S.U.: sravanti.uppaluri@apu.edu.in, C.P.B.: cbrangwy@princeton.edu

1 Supplementary Experimental Data

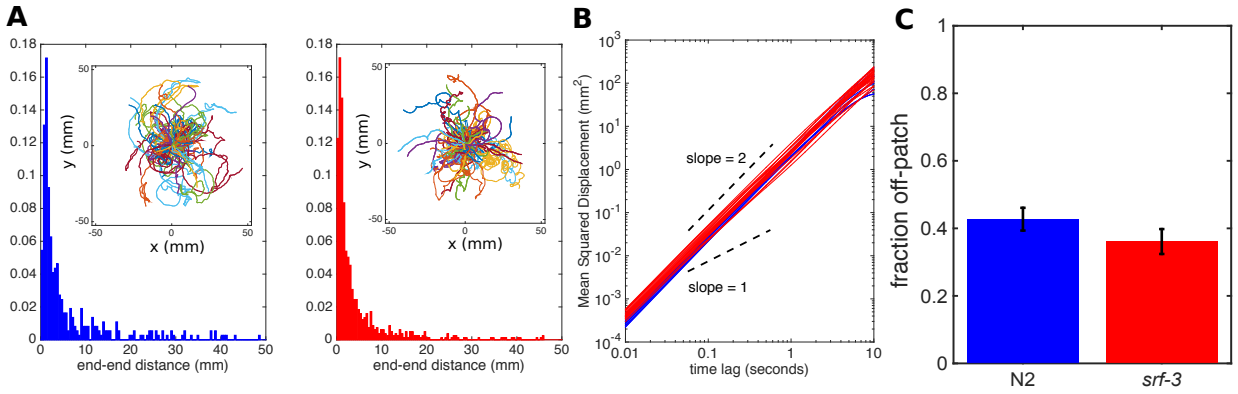

Figure S1: **A**. Trajectory analysis of farmer/wild type worms (blue data, $n = 400$ tracks) and non-farmer/*srf-3* mutant (red data, $n = 400$ tracks) showing the distribution of end-end distances of multiple trajectories obtained by tracking 10 worms on a bacteria-free agar surface of each type over a period of 4 hours. **B.** The mean squared displacements for the trajectories shown in panel **A.** Red curves represent the non-farmer/*srf-3* worm data and the blue curves represent the farmer/wild type worm data. This is on time scales shorter than the reproduction time of the worms. Data for 20 trajectores is shown. **C.** Fraction of worms by genotype that have moved off the patch of bacteria. 20 independent experiments, totaling ∼2000 worms.

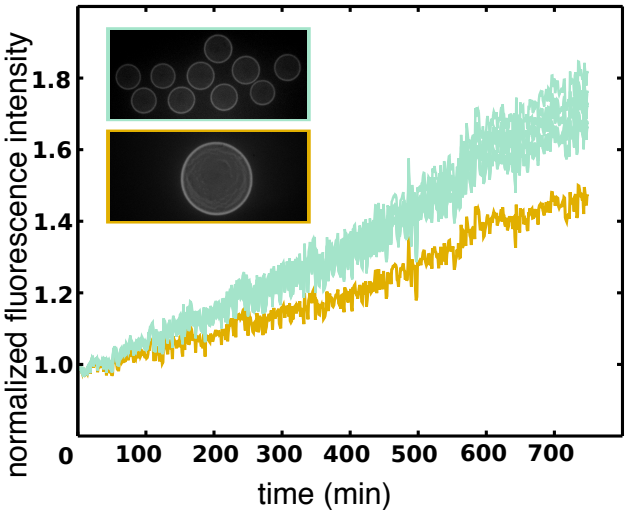

Figure S2: Bacteria distributed in smaller patches grow faster than when compared to the same experiment with one big patch.

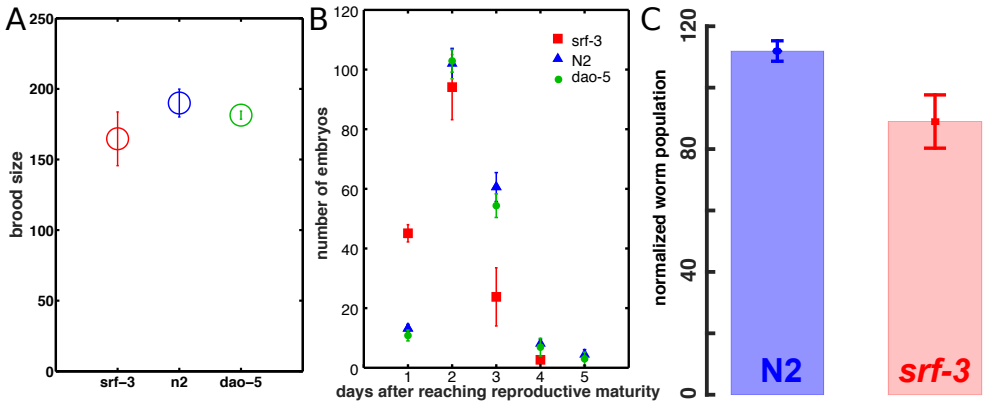

Figure S3: **A**. Mean brood size (progeny per worm life time) for each genotype ($n = 10$ for each genotype). These measurements were made in a controlled setting where farming was inhibited by covering the entire plate with a uniform bacterial lawn. **B**. Eggs laid over time for each genotype. **C** Worm population sizes as shown in main text **Fig. 2C** normalized by respective brood size.

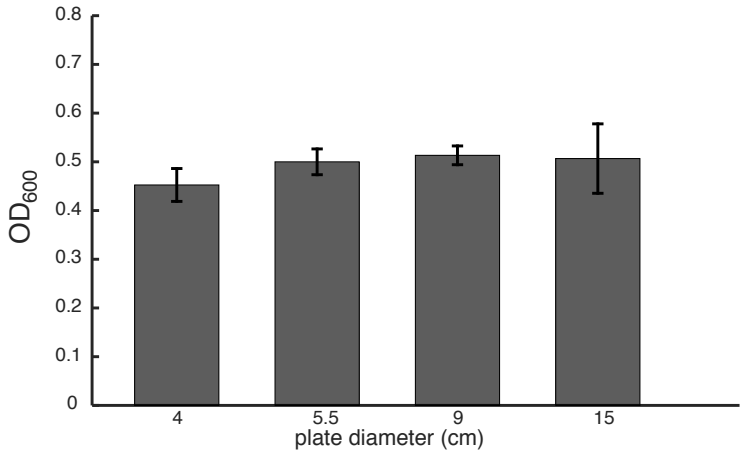

Figure S4: Bacterial growth on petri dishes of different sizes. Optical density (OD_{600}) of bacteria washed off after 48 hours from plates of different diameters with the same initial bacterial seed ($n = 4$ for each time point).

2 Theoretical modeling

We develop a spatially implicit model of *C. elegans* and their bacterial farming behavior. Because very little is known about the worm spatial behavior and the wide gamut of exploitation-exploration strategies employed, the model encapsulates these ideas phenomenologically based on physically- and experimentally-grounded assumptions. Therefore, we do not expect quantitative agreement with the data; rather we aim for qualitative agreement in the context of a simple enough, but physically and biologically-grounded, model that can allow us to test our proposed farming mechanism but also to explore different scenarios and make testable predictions.

Bacteria. Because the feeding and farming behaviors of the worms will be assumed (see below) to affect the area and density of bacteria in ways that can not be captured by the total number of bacteria alone, our model describes the bacteria in terms of its area A_B and density, ρ, instead of using only the total number, B. Of course, the number is determined by these quantities as $B = \rho A_B$. The bacterial growth dynamics in the absence of worms is given by

$$\frac{dA_B}{dt} = g_A A_B \left(1 - \frac{A_B}{\pi R^2}\right), \tag{S.1}$$

$$\frac{d\rho}{dt} = g_\rho \rho \left(1 - \frac{\rho}{K_\rho}\right). \tag{S.2}$$

Here R is the plate radius. The logistic growth captures the experimentally observed behavior that less-dense patches grow faster than dense patches. Parameters g_A, g_ρ and K_ρ are fitted to experimental measurements of the bacterial growth (see Table S1).

Worms. Worms feed on bacteria to grow and reproduce. The worm feeding rate is dependent on the number of bacteria available, the spatial distribution of the bacteria (characterized here by A_B) and the total plate area, πR^2. For simplicity of notation we will write it as $F(A_B, \rho, R)$ to denote that it depends on bacterial and plate characteristics. We describe it via a Holling's type II function, which is a natural ecological assumption

$$F(A_B, \rho, R) = \frac{c\,\Psi\left(A_B, R\right)\rho A_B}{1 + c\,\Psi\left(A_B, R\right)\rho A_B}, \tag{S.3}$$

with a modified attack/encounter rate

$$\Psi(A_B, R) = \exp\left(-\frac{\pi R^2}{\sigma A_B}\right). \tag{S.4}$$

The parameter c controls the rate of increase of the feeding rate with the amount of bacteria available. Our choice of $\Psi\left(A_B, R\right)$ is phenomenological but could be experimentally fitted from the analysis of worm movement. Under the assumption that the encounter rate decreases with large plate size or low available bacteria, we choose $\Psi\left(A_B, R\right)$ to be the modified Gaussian function above. The parameter σ controls how quickly (and at what plate radius

relative to bacterial area) the worm-bacteria encounter rate drops off as the plate radius increases.

Although this constitutes a reasonable choice in the absence of additional mechanistic information on worm space-use, it is important to note that this choice will make quantitative agreement between theory and data unlikely. For instance, on large plates it is likely that memory plays a role in restricting the movement of the worms from the bacteria-rich center of the plate, so that the encounter might not decrease as quickly at large plate sizes as this functional form suggests. Similarly, at early times, the spatial distribution of the initial worm and its progeny on the plate are likely to matter: while it may be true that the encounter rate decreases with plate size for an average worm hatching at some random position on the plate, this is likely untrue for the first worm that is placed initially in the bacteria-rich center of the plate. In turn, the progeny of this first worm may be laid close to the central bacteria patch and also experience a non-average encounter rate. While at longer times over the course of the experiment these spatial correlations may become muted (as eggs are laid further from the center of the plate), our spatially implicit model will fail to capture these early time spatial effects, which could cause quantitative though as we will show not qualitative differences between the theoretical and experimental long time behavior of the near-exponentially growing worm population.

Effect of worms on bacteria: Feeding. The number of bacteria decrease proportional to the worm feeding rate; however, we need to make some assumptions about how the worm feeding may affect the spatial distribution and density of the bacteria. We assume that the area is preserved, but the density is decreased. Essentially this assumes that the bacteria maintains some of the spatial distribution from its growth phase, but becomes ever more diffuse or 'patchy'.

Effect of worms on bacteria: Farming. We expect that the farming behavior will increase the area of the bacteria, decrease the density, but preserve the total amount of bacteria. We introduce a spreading function and we assume that the rate of spreading is proportional to the encounter rate $\Psi(A_B, R)$, and to the amount of free space on the plate (spreading the bacteria is impossible if there is no free space); furthermore, we assume that it increases linearly with the density of the bacteria (worms are less likely to pick up bacteria when it is thinly spread). For simplicity of notation we denote this function by $S(A_B, \rho, R)$ to show its dependence on bacterial and plate characteristics:

$$S(A_B, \rho, R) = s\,\psi(A_B, R)\,\rho\left(\pi R^2 - A_B\right)\,, \tag{S.5}$$

where s is a constant (see Table S1).

2.1 Spatially-implicit model

Based on the discussion above, a model able to capture the worm-bacteria dynamics will have at least three variables, two accounting for the area and density of bacteria and one

accounting for the worms. The worms, W, reproduce at a rate proportional to the feeding rate $F(A_B, \rho, R)$, Eq. (S.3), with a conversion factor ϵ. The model then becomes:

$$\begin{aligned}
\frac{dA_B}{dt} &= g_A A_B \left(1 - \frac{A_B}{\pi R^2}\right) + \frac{A_B}{\rho} S(A_B, \rho, R) W \,, \\
\frac{d\rho}{dt} &= g_\rho \rho \left(1 - \frac{\rho}{K_\rho}\right) - \frac{a}{A_B} F(A_B, \rho, R) W - S(A_B, \rho, R) W \,, \qquad \text{(S.6)} \\
\frac{dW}{dt} &= \epsilon F(A_B, \rho, R) W \,. \qquad \text{(S.7)}
\end{aligned}$$

The parameter s is zero for non-farming srf-3 and greater than zero for farming N2 worms.

Parameter estimation. This spatially-implicit model has eight parameters. The parameters associated with the bacterial growth in the absence of worms, g_A, g_ρ and K_ρ, can be fitted experimentally. This leaves five parameters associated with the worm: a, ϵ, c, σ and s. Three of these, c, σ and s are parameters related to the phenomenological feeding rate $F(A_B, \rho, R)$, and the spreading rate, and they are difficult to fit experimentally. The remaining two parameters a and ϵ do not have unambiguous, measurable analogues in the experimental system. For instance the maximum feeding rate parameter, a, represents the maximum rate at which bacteria is converted into the class 'worms'; however, experimentally, this worm class includes *C. elegans* eggs that neither eat nor reproduce, *C. elegans* juveniles that consume bacteria but do not reproduce, and *C. elegans* adults that both consume bacteria and reproduce. It is therefore not possible to determine a suitable choice for a that appropriately weights each of these life stages, especially when the system is far from equilibrium.

Qualitative agreement with data. Thus, although this version of the model is minimal in terms of the number of variables, it has the downside that most parameters can not be experimentally-inferred. Nevertheless, it can be useful to explore the parameter space and determine (i) the ability of this model and its underlying assumptions to qualitatively capture the experimental observations, and (ii) the robustness of that qualitative agreement. Using this model, we study the dynamics of the farmer, N2 and non-farmer, srf-3 phenotypes independently. We assume that the two types have identical foraging behavior but differ in their ability to spread bacteria. Therefore, we pick c and σ to be the same for both phenotypes but let s be zero for non-farmers and non-zero for farmers. This captures the two types used in our experiments. We allow the five free parameters a, ϵ, c, σ and s to vary and scan parameter space to identify parameters that yield a qualitative agreement between theory and experiment (see Supplementary Movie 5). A reasonable qualitative agreement with experimental data can be found for a broad range of parameter values, as illustrated in Figure S5. In this figure, the parameters have been chosen to illustrate the qualitative agreement between theory and experiment; furthermore, since the worm count is measured experimentally at the time of collapse of the bacterial population on the smallest plate ($t = 144$ hours on the $R = 2$ cm plate), model parameters have also been chosen in such a way that the model results give a similar time of collapse (see Figure S5, lower panel).

Quantitative fit. However, as expected, we note the poor quantitative agreement: this

model overestimates the number of worms in the population by a factor 40. We also note that while it predicts that larger N2 plates do experience enhanced bacterial growth, the model under-predicts the magnitude of this enhancement when compared to that measured experimentally. Although we expected that a spatially-implicit model that only phenomenologically captures details of worm space-use can not give a quantitative fit, there is an additional reason for the large overestimate, a reason which also underlies the inability to fit most of the parameters of this model: the model contains a single worm class, in which the worms are always reproductively capable and produce more reproductively capable worms. This misses the fact that worms lay eggs that take time to hatch and produce sexually immature worms; the latter take time to mature and be able to reproduce; eventually, they become infertile. There are behavioral differences between these age classes that warrant individual descriptions of their dynamics: eggs do not move, consume resources or reproduce; sexually immature worms move, consume resources but do not reproduce; sexually mature worms engage in all behaviors; infertile worms have ceased to reproduce. With one worm class, parameters that reflect reproduction, movement or feeding are necessarily taken to be time averages of the combined population and can not quantitatively capture its dynamics.

2.2 Age-structured spatially-implicit model

In this section we retain the simplicity of the previous model but add age structure to more accurately capture the worm dynamics; this is the full model discussed in the main text. Here we have four worm classes: eggs, W_E, sexually immature worms, W_I, sexually mature worms, W_M, and infertile worms, W_D. The distinct nature of these life stages makes it easier to obtain, directly or from existing literature, experimental estimates on the transition rates between the life stages, for instance the time it takes for an egg to hatch, or the maximum rate at which a juvenile worm can reach sexual maturity (see Table S1).

In the age-structured model, eggs hatch at a constant rate $1/\tau_{hatch}$. Immature, mature and infertile worms all feed. Immature worms do not lay eggs but mature at a rate that depends on their food intake, with a conversion factor ϵ_1. Sexually mature worms lay eggs at a rate that depends on their food intake, with a conversion factor ϵ_2. Sexually mature worms additionally become infertile at a rate proportional to their food intake (and therefore the number of eggs they have laid) with a conversion factor d. Finally, we assume that for the farming N2 worms, only sexually mature and infertile worms are large enough to contribute to the spreading of bacteria.

Overall, the dynamics of the system is described by the following set of ODEs:

$$\begin{aligned}
\frac{dA_B}{dt} &= g_A A_B \left(1 - \frac{A_B}{\pi R^2}\right) + \frac{A_B}{\rho} S(A_B, \rho, R)(W_M + W_D)\,, \\
\frac{d\rho}{dt} &= g_\rho \rho \left(1 - \frac{\rho}{K_\rho}\right) - \frac{a}{A_B} F(A_B, \rho, R)(W_I + W_M + W_D) - S(A_B, \rho, R)(W_M + W_D)\,, \\
\frac{dW_E}{dt} &= \epsilon_1 F(A_B, \rho, R) W_M - \frac{1}{\tau_{hatch}} W_E\,, \\
\frac{dW_I}{dt} &= \frac{1}{\tau_{hatch}} W_E - \epsilon_2 F(A_B, \rho, R) W_I\,, \\
\frac{dW_M}{dt} &= \epsilon_2 F(A_B, \rho, R) W_I - d F(A_B, \rho, R) W_M\,, \\
\frac{dW_D}{dt} &= d F(A_B, \rho, R) W_M\,.
\end{aligned} \tag{S.8}$$

Parameter estimation. We obtained experimental estimates for the majority of our parameters (see Table S1), such that the only free parameters are those related to the phenomenological feeding rate, c, σ and the spreading rate, s. Thus, although the previous version of the model was simpler in the sense that it had the minimal number of variables needed to capture the bacteria-worm interaction, this age-structured version has a much smaller number of free parameters.

Qualitative agreement with data. Using this age-structured spatially-implicit model, we study, as before, the dynamics of the farmer, N2 and non-farmer, srf-3 phenotypes independently. We assume that the two types have identical foraging behavior but differ in their ability to spread bacteria. Therefore, we pick c and σ to be the same for both phenotypes but let s be zero for non-farmers and some positive value for farmers. This captures the two types used in our experiments. We find very good qualitative agreement with the experimental results (Figure S7). We note that the worm numbers resulting from the ODEs have been rescaled (here by a factor of 4) for easier qualitative comparison with the experimental results. The robustness of these results to varying the free parameters in the model is explored in Supplementary Movie 3. Figure S6 further shows the good qualitative agreement in worm number; however it also captures the dependence of the result on the time at which the worm numbers are counted. In the experiments, the worm count was recorded at $t = 144$ hours, the time at which the bacterial population collapsed on the smallest plate ($R = 2$cm) for both N2 and srf-3 worms. In order to align the model results more easily with those obtained experimentally, we have chosen parameters that give the same time of collapse of the bacterial population (see Figure S6). As parameters are varied in the model, this time of collapse will also change. The effect of varying the free parameters on the bacterial dynamics is demonstrated in Supplementary Movie 4. Figure S8 shows how the maximum amount of bacteria across infinite times changes with plate size and worm type. Farming significantly increases the amount of bacteria available.

Quantitative fit. Promisingly, the age-structured spatially-implicit model also provides a quantitative improvement on the previous version of the spatially-implicit model, being

only a factor 4 larger than the experimental values for absolute worm number (see Figures 3 and S7), compared to the factor 40 difference found previously (see Figure S5). It is important to note, however, that even with this extended version of the model, there are still experimental parameters that do not cleanly map onto our theoretical parameters. For instance, our experiments indicate that there are phenotypic differences in the time at which eggs are laid between the srf-3 and N2 worms (see Figure S3): although N2 lay more eggs in absolute terms, srf-3 lay their eggs more rapidly. These differences in number versus speed can not be accounted for with our single egg-laying rate parameter, ϵ_2; this could be solved by including additional worm classes (e.g. sexually mature on day 1, sexually mature on day 2 etc.) but that would further complicate the model without significant additional advantage (while it could lead to an even better quantitative fit, we never expect that fit to be perfect due to the phenomenological aspects). We therefore made a concession to simplicity and decided to approximate ϵ_2 for both genotypes to be equal to their joint average egg-laying rate. Similarly, other parameters, such as feeding rate, egg-laying rate and bacteria spreading rate are likely to vary continuously across worm development. Our model, with only four distinct life stages, does not account for this, primarily because we lack data on how these changes in worm behavior vary continuously with development. Since due to the phenomenological nature of the fitting rate we do not expect quantitative agreement anyway, such an increase in model complexity to reflect a more continuous development is unwarranted since it would not yield a significant quantitative improvement and it would be riddled with parameters that are hard to estimate. Therefore, we henceforth work with the full model above, which has a very small number of free parameters and is sufficiently simple to be useful.

2.2.1 Competition between farmers and non-farmers: same foraging behavior and no additional cost of farming; Figures S9 and S10

In this section we use the age-structured spatially-implicit model to study the dynamics of a mixed system with both farmers and non-farmers competing for the same resource, the bacteria. As above, we assume the the farmers and non-farmers have the same behavior and differ only in their ability to farm (i.e. their stickiness). This setup mirrors our experimental competition setup and the analysis in this section is meant to test whether the assumption that farming is a public good can explain the observed experimental behavior. The ODE

system becomes:

$$
\begin{aligned}
\frac{dA_B}{dt} &= g_A A_B\left(1-\frac{A_B}{\pi R^2}\right)+\frac{A_B}{\rho}S(B,R)\left(W_M^{(N2)}+W_D^{(N2)}\right),\\
\frac{d\rho}{dt} &= g_\rho\rho\left(1-\frac{\rho}{K_\rho}\right)-\frac{a}{A_B}F(A_B,\rho,R)\left(W_I^{(srf3)}+W_M^{(srf3)}+W_D^{(srf3)}+W_I^{(N2)}+W_M^{(N2)}+W_D^{(N2)}\right)\\
&\quad -S(B,R)\left(W_M^{(N2)}+W_D^{(N2)}\right),\\
\frac{dW_E^{(srf3)}}{dt} &= \epsilon_1 F(A_B,\rho,R)W_M^{(srf3)}-\frac{1}{\tau_{hatch}}W_E^{(srf3)},\\
\frac{dW_I^{(srf3)}}{dt} &= \frac{1}{\tau_{hatch}}W_E^{(srf3)}-\epsilon_2 F(A_B,\rho,R)W_I^{(srf3)},\\
\frac{dW_M^{(srf3)}}{dt} &= \epsilon_2 F(A_B,\rho,R)W_I^{(srf3)}-dF(A_B,\rho,R)W_M^{(srf3)},\\
\frac{dW_D^{srf3}}{dt} &= dF(A_B,\rho,R)W_M^{srf3},\\
\frac{dW_E^{(N2)}}{dt} &= \epsilon_1 F(A_B,\rho,R)W_M^{(N2)}-\frac{1}{\tau_{hatch}}W_E^{(N2)},\\
\frac{dW_I^{(N2)}}{dt} &= \frac{1}{\tau_{hatch}}W_E^{(N2)}-\epsilon_2 F(B,R)W_I^{(N2)},\\
\frac{dW_M^{(N2)}}{dt} &= \epsilon_2 F(A_B,\rho,R)W_I^{(N2)}-dF(A_B,\rho,R)W_M^{(N2)},\\
\frac{dW_D^{N2}}{dt} &= dF(A_B,\rho,R)W_M^{N2}.
\end{aligned}
$$

The ratio of the final number of srf-3 and N2 worms, as a function of the initial fraction of the two phenotypes, is plotted in Figure S10. While the general linear trend of the experimental results is captured, the precise slope is not (see Figure 4A). This is in part because the model does not capture the experimental result that on small plates the farming N2 worms exist as smaller numbers on the $R = 2.75cm$ plates than the non-farming srf-3 worms. Consequently, the increase in the number of N2 worms between the $R = 2.75cm$ and $R = 7.5cm$ plates is less in the model than that observed experimentally, resulting in the decreased slope in Figure S10.

2.3 Theoretical explorations and new predictions

Here we use the age-structured spatially-implicit model developed in Section 2 to investigate the system dynamics under several scenarios and make predictions for future experimental work.

2.3.1 Competition between farmers and non-farmers – same foraging behavior but mortality cost for farmers due to pathogenic bacteria; Figure S11

The N2 phenotype, by virtue of its ridged skin, is more susceptible to picking up bacteria, including pathogenic types that are likely to kill it. We propose that this might constitute an indirect cost associated with farming. In order to investigate this idea, we add an additional rate of death to N2 worms in the population. The 'infection' of N2 worms with pathogenic bacteria occurs when food that the worm has trapped around its face/body begins to form a biofilm around the worm's face, suffocating it. We might therefore expect the rate of 'infection' to be proportional to both the bacterial encounter rate and bacterial density. With this is mind, we introduce a death rate due to pathogenic bacteria $\delta\psi(A_B, R)\rho$. The competition equations are the same as in the previous section, except those for the farmer worms which are now modified to account for the extra mortality:

$$\begin{aligned}
\frac{dW_I^{(N2)}}{dt} &= \frac{1}{\tau_{hatch}} W_E^{(N2)} - \epsilon_2 F(A_B, \rho, R) W_I^{(N2)} - \delta\psi(A_B, R)\rho W_I^{(N2)}\,, \\
\frac{dW_M^{(N2)}}{dt} &= \epsilon_2 F(A_B, \rho, R) W_I^{(N2)} - dF(A_B, \rho, R) W_M^{(N2)} - \delta\psi(A_B, R)\rho W_M^{(N2)}\,, \\
\frac{dW_D^{(N2)}}{dt} &= dF(A_B, \rho, R) W_M^{(N2)} - \delta\psi(A_B, R)\rho W_D^{(N2)}\,,
\end{aligned}$$

We find that the increased mortality affects the farmer population negatively and creates an advantage for the non-farmers who can take advantage of the farming without incurring the mortality cost. One additional point worth noting is that the death-by-pathogen rate lowers the effective growth rate of the N2 worm population. In turn, this lowers the rate of increase of the population. During this time, the bacteria has the opportunity to grow to greater abundances. Thus the pathogenic death rate of N2 worms can, in isolation, actually result in an increased overall number of worms relative to the case of no pathogenic death for the N2s. When N2 competes with srf-3, the slowed N2 growth does not result in additional bacterial growth, since this is simply consumed by the srf-3 (see Figure S11).

2.3.2 Competition between two farmers – different foraging behaviors; Figure S12 and S13

In this spatially implicit model, it is difficult to capture explicitly the dynamics of different foraging strategies. However, we can capture this implicitly. The encounter rate $\psi(A_B, R)$ measures how effective the worms are at foraging: a low σ means that the encounter rate decreases rapidly with the amount of empty space on the plate and could be interpreted as an inefficient search strategy, or even a poor memory resulting in the worms getting lost often; a high σ indicates a very good search strategy, or a good memory (the encounter rate is not affected by plate size because the worms find bacteria quickly either due to efficient foraging or due to good memory). In addition to σ, the egg-laying rate ϵ_1 can be used as a proxy for a cost to improved foraging. A worm with a reduced ϵ_1 reproduces more slowly than its counterpart in the presence of the same amount of bacteria. A high σ, low ϵ_1 worm then

forages very efficiently, (space does not affect its feeding rate) but responds to what it does find less efficiently. Arguably this could be interpreted as the metabolic cost paid for more time spent foraging around the plate rather than staying in one location and consuming the bacteria there. Here we investigate what can happen if we vary σ and ϵ_1.

We consider two worms denoted 1 and 2 and for $i = 1, 2$ we write:

$$F^{(i)}(A_B, \rho, R) = \frac{c\,\Psi^{(i)}(A_B, R)\,A_B\rho}{1 + c\,\Psi^{(i)}(A_B, R)\,A_B\rho}\,, \qquad \Psi^{(i)}(A_B, R) = \exp\left(-\frac{\pi R^2}{\sigma_i A_B}\right)\,, \tag{S.9}$$

and

$$S^{(i)}(A_B, \rho, R) = s\,\rho\left(\pi R^2 - A_B\right)\Psi^{(i)}(A_B, R) \tag{S.10}$$

The modified competition equations take the form:

$$\begin{aligned}
\frac{dA_B}{dt} &= g_A A_B\left(1 - \frac{A_B}{\pi R^2}\right) + \frac{A_B}{\rho}\left(S^{(1)}(B,R)W_M^{(1)} + S^{(2)}(B,R)W_M^{(2)}\right)\,,\\
\frac{d\rho}{dt} &= g_\rho\rho\left(1 - \frac{\rho}{K_\rho}\right) - \frac{a}{A_B}\left[F^{(1)}(B,R)\left(W_I^{(1)} + W_M^{(1)}\right) + F^{(2)}(B,R)\left(W_I^{(2)} + W_M^{(2)}\right)\right]\\
&- \left[S^{(1)}(B,R)W_M^{(1)} + S^{(2)}(B,R)W_M^{(2)}\right]\,,\\
\frac{dW_E^{(1)}}{dt} &= \epsilon_1^{(1)}F^{(1)}(B,R)W_M^{(1)} - \frac{1}{\tau_{hatch}}W_E^{(1)}\,,\\
\frac{dW_I^{(1)}}{dt} &= \frac{1}{\tau_{hatch}}W_E^{(1)} - \epsilon_2 F^{(1)}(B,R)W_I^{(1)}\,,\\
\frac{dW_M^{(1)}}{dt} &= \epsilon_2 F^{(1)}(B,R)W_I^{(1)} - dF^{(1)}(A_B,\rho,R)W_M^{(1)}\,,\\
\frac{dW_D^{(1)}}{dt} &= dF^{(1)}(A_B,\rho,R)W_M^{(1)}\,,\\
\frac{dW_E^{(2)}}{dt} &= \epsilon_1^{(2)}F^{(2)}(B,R)W_M^{(2)} - \frac{1}{\tau_{hatch}}W_E^{(2)}\,,\\
\frac{dW_I^{(2)}}{dt} &= \frac{1}{\tau_{hatch}}W_E^{(2)} - \epsilon_2 F^{(2)}(B,R)W_I^{(2)}\,,\\
\frac{dW_M^{(2)}}{dt} &= \epsilon_2 F^{(2)}(B,R)W_I^{(2)} - dF^{(2)}(A_B,\rho,R)W_M^{(2)}\,,\\
\frac{dW_D^{(2)}}{dt} &= dF^{(2)}(A_B,\rho,R)W_M^{(2)}\,.
\end{aligned}$$

In what follows worm 2 will be our $N2$ farmer above such that $\epsilon_1^{(2)} = \epsilon_1$ and $\sigma^{(2)} = \sigma$, with ϵ_1 and σ as in the previous sections. Parameters $\epsilon^{(1)}$ and $\sigma^{(1)}$ pertaining to a hypothetical worm $N1$ will be varied. In Figure S12 and S13 we plot the results of the simulation, for a case in which improved foraging incurs a cost, and a case where it does not.

In this scenario, we find that the benefits accrued from improved foraging are strongly

dependent on plate size. The form of the encounter rate, Eq. (S.9), together with the typical values for $\sigma^{(2)}$ (which we infer from experimental observation, see Table S1), mean that the benefits of improved foraging are muted on small plates and become more prominent as plate size is increased. This can be physically interpreted as implying that distinct foraging strategies lead to encounter rates that differ little on small plates and differ more significantly as the amount of free space on the plate is increased (see Figures S12 and S13).

If the cost to N1 of improved foraging is too high, it is possible for N1 worms to be out-competed (see Figure S12), while if the cost of foraging is small or non-existent, the N1 can out-compete N2 (see Figure S13). In Section 2.3.1, we discussed the counter-intuitive observation that in homogeneous monocultures costs to phenotypes can be beneficial at the population level by releasing pressure on the food resource (bacteria). Similar results hold here (see right panel of Figure S12 and all panels in Figure S13). However, it must be noted that the general observation that "worms that fare worse in competition are comparatively better in isolation" does not always hold; in Figure S12, left panel, the cost of foraging to the N1 worm's reproduction is sufficiently high, and the benefits from foraging sufficiently muted on the small plate, that N1 worms are slightly inferior to N2 worms both in competition and isolation.

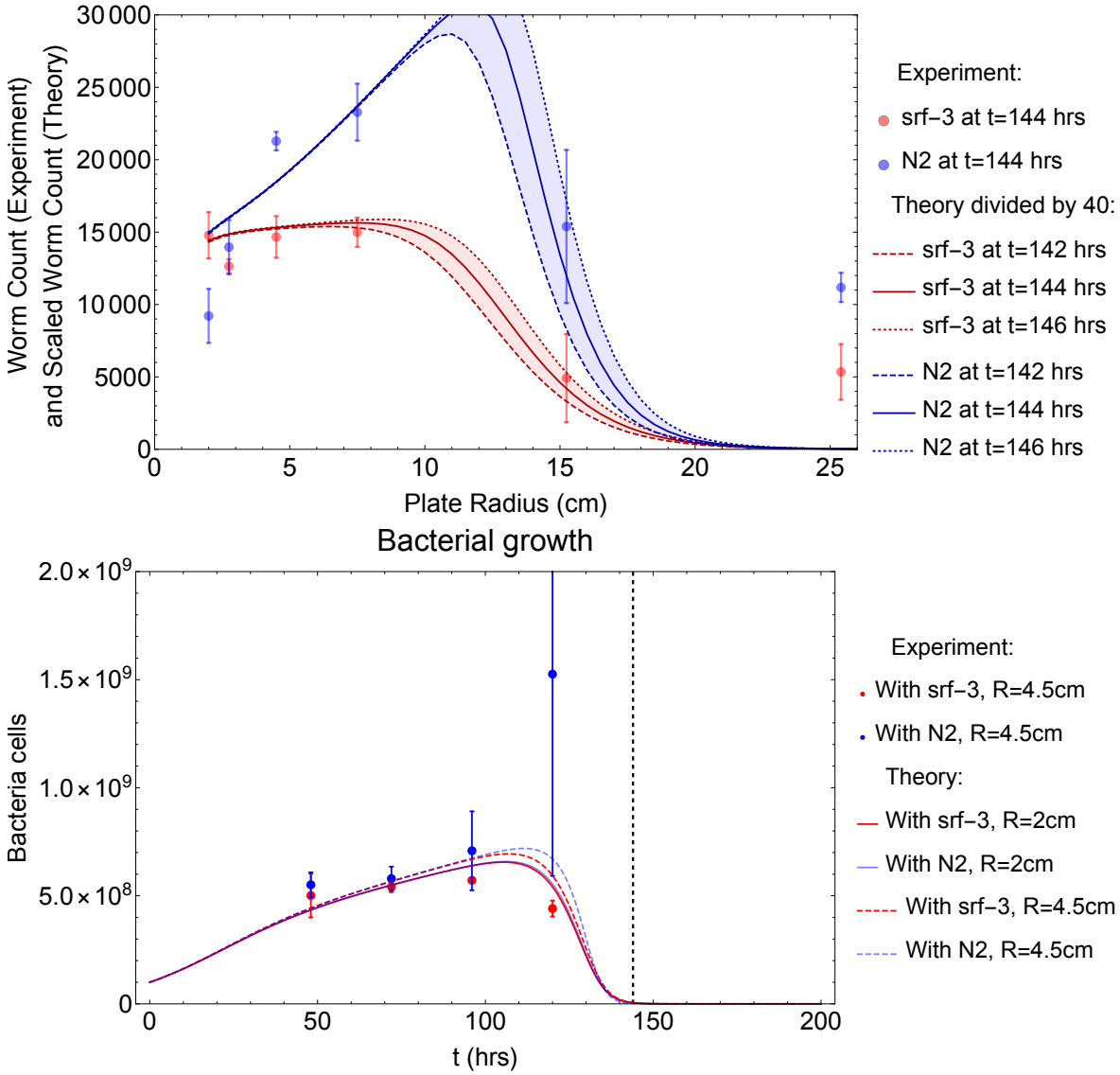

Figure S5: Results from the non-age-structured spatially-implicit model (see Section 2.1). Top panel: Worm count at $t = 144$ hrs as a function of plate size in the model. Dashed lines enclose worm counts at $t = 144 \pm 2$ hrs. Bottom panel: Experimental measurements (markers) and theoretical curves (solid lines) for the bacterial growth on the smallest plate, $R = 2\,\text{cm}$. For both panels, red plots are associated with non-farming srf-3 worms, and blue plots with farming N2 worms. Bacterial growth parameters (g_A, g_ρ and K_ρ) are taken from Table S1. Remaining parameters used are $a = 8$ cells/min, $\epsilon = 4.5 \times 10^{-3}$ min^{-1}, $c = 1.4 \times 10^{-9}$ cells^{-1}, $\sigma = 1200$ cm^2 and $s = 1 \times 10^{-10}$ min^{-1}cm^{-2}. The ODE results for the worm number are divided by 40 for comparison with experimental results. Similar plots are presented in Supplementary Movie 5, where each of the parameters is varied over a range of values.

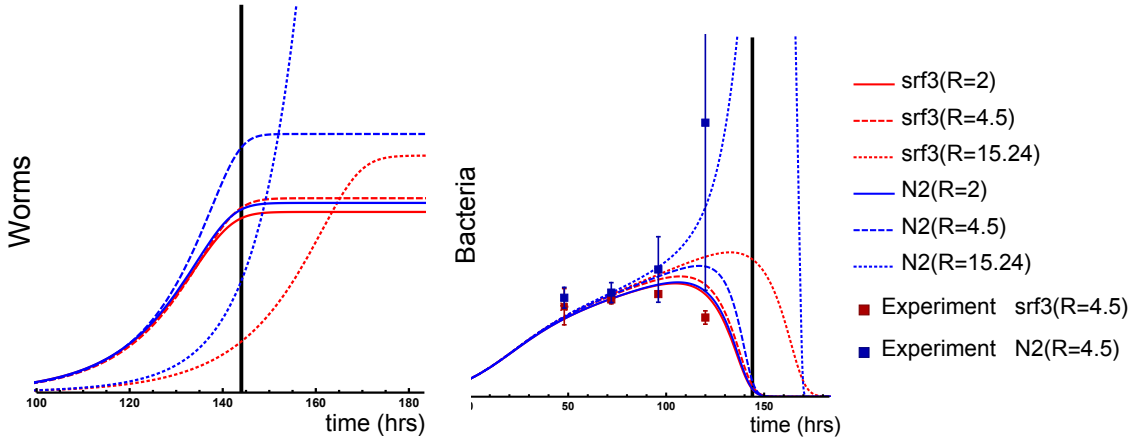

Figure S6: Individual behavior of farmers versus non-farmers in the age-structured spatially-implicit model. Total number of worms ($W_E + W_I + W_M + W_D$) and number of bacteria ($B = A_B\rho$) from the model, shown as a function of time. Parameters taken from Table S1, while s is 0 for non-farming srf-3. Blue curves represent plates with farmers (N2); red curves represent plates with non-farmers (srf-3). The black vertical line represents the time point at which the worm numbers are counted in experiments. Initial conditions: $W_E(0) = W_I(0) = 0$, $W_M(0) = 1$ and $W_D = 0$ for both worms. Overall, farming increases worm number: at shorter time scales (such as the time used for experimental measurements), worms do better on intermediate sized plates because on large plates they do not encounter bacteria as regularly; however, on longer time scales, the bigger the plate, the larger the worm population. This gives good qualitative agreement with the experiments and shows the importance of the time at which worm numbers are compared. The model results show the trajectories that could not be measured experimentally.

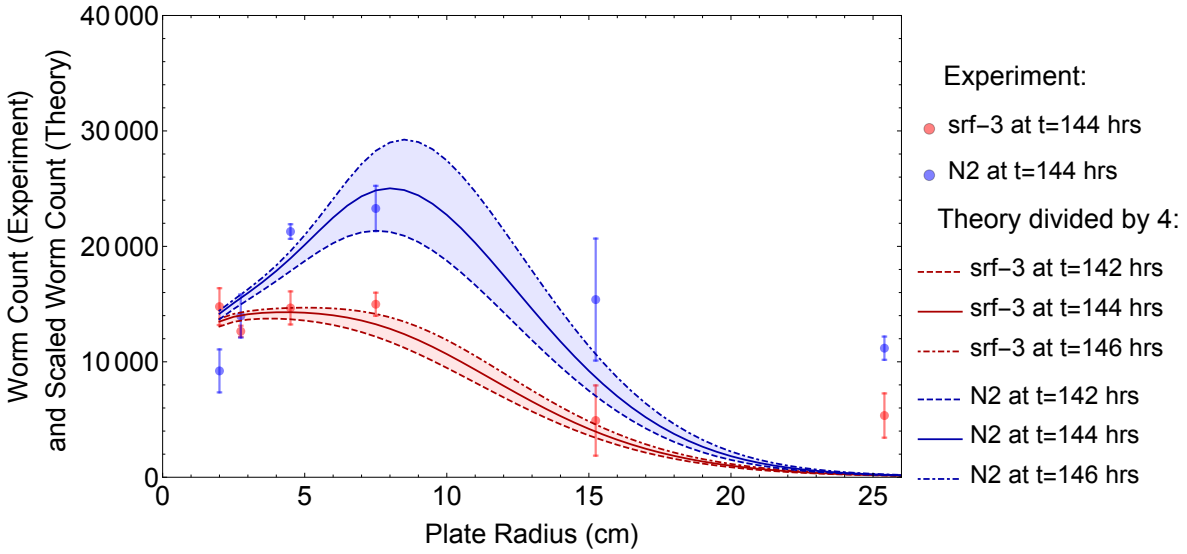

Figure S7: Worm count as a function of plate size in the age-structured, spatially implicit model. Parameters are given in Table S1. Worms are identical in all respects except farming. ODE results divided by 4 to facilitate visual qualitative comparison with experimental results.

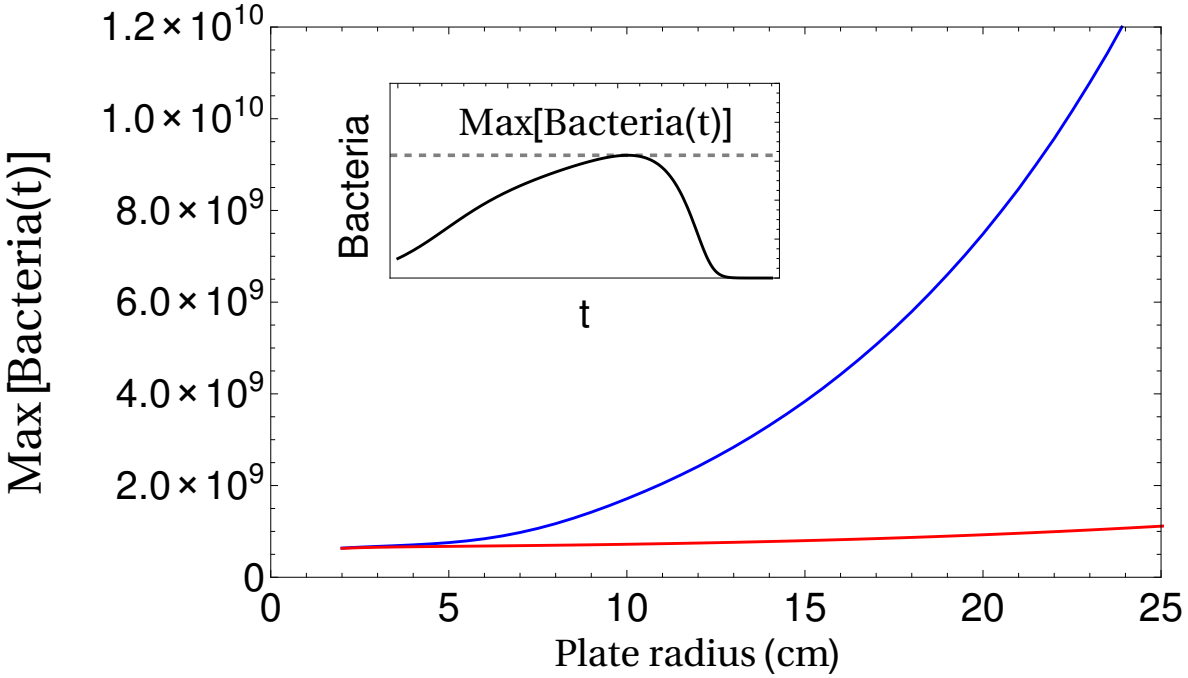

Figure S8: Results of the age-structured spatially-implicit model showing the maximum amount of bacteria present on a plate at any time as a function of plate radius. Plates with srf-3 worm populations are plotted in red: A slight increase in the maximum amount of bacteria is observed as plate size increases, as the bacteria-worm encounter rate is diminished on larger plates, leading to a lower bacteria consumption rate at short times. Plates with N2 worm populations are plotted in blue: The act of farming creates a much larger increase in the maximum amount of bacteria observed as a function of plate size.

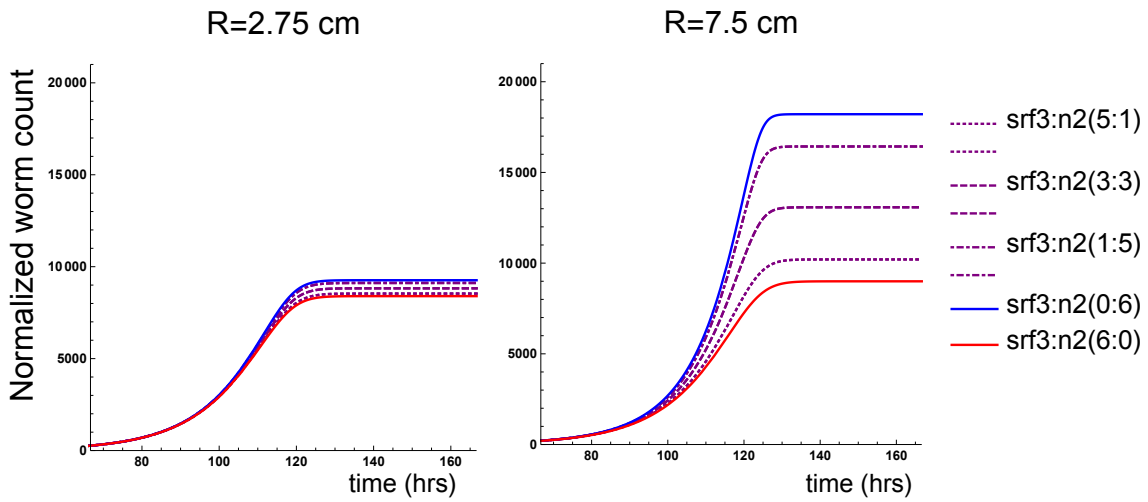

Figure S9: In the absence of fitness costs associated with farming, both worm phenotypes use the public good equally. Worm counts for each phenotype, normalized by the initial worm number of the respective phenotype. Blue = only N2, red = only srf-3, starting with $W_E(0) = W_I(0) = 0$, $W_M(0) = 6$ and $W_D(0) = 0$. Purple curves = mixtures of srf-3 and N2; when normalized by the initial condition, the two worms have identical growth rates. Overall, srf-3 uses the public good to boost its numbers; the more producers there are in the population, the better srf-3 fares. In mixed populations, N2 fares worse than in isolation; the more srf-3 there are, the lower the final total population number. Left panels: plate of size $R = 2.75$ cm; right panels = plate of size $R = 7.5$ cm.

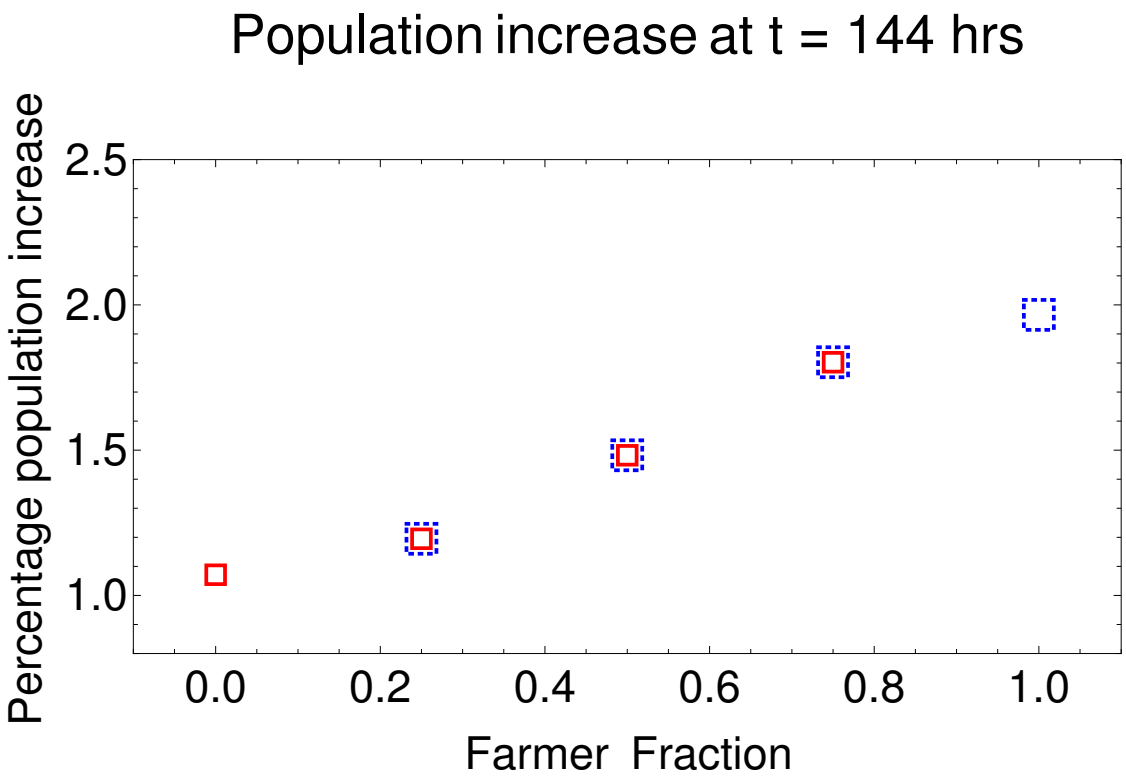

Figure S10: Red (blue) squares = ratio between srf-3 (N2) worm count on a plate of size $R = 7.5$ versus a plate of size $R = 2.75$, taken at time $t = 144$ to allow comparison with the experiments. Measurements are taken under various initial ratios of srf-3 and N2 corresponding to the curves in Figure S9: 6 SRF-3 worms and 0 N2; 5 SRF-3 worms and 1 N2; 3 SRF-3 and 3 N2; 1 SRF-3 and 5 N2; and finally 0 SRF-3 and 6 N2.

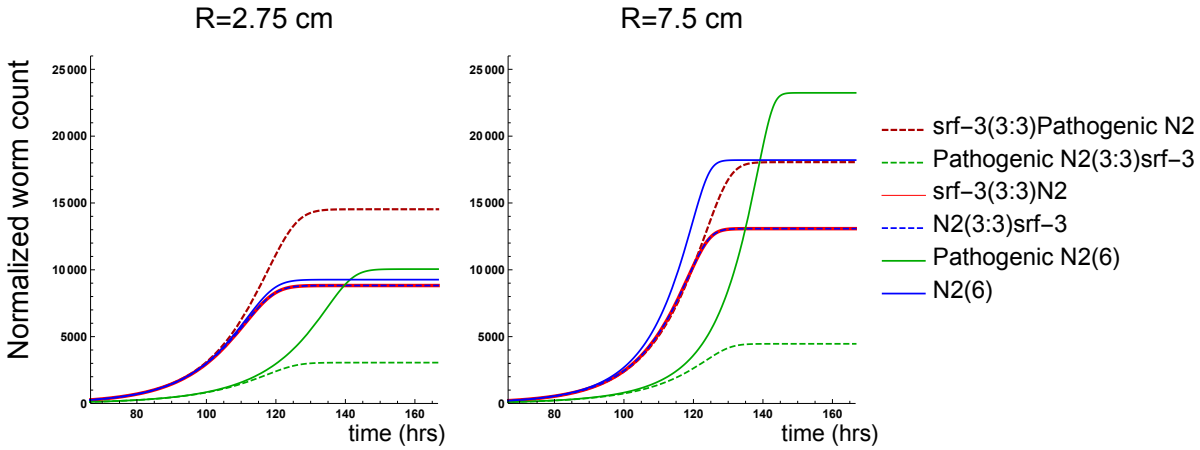

Figure S11: Increased mortality associated with farming behavior leads to the farmer being out-competed by non-farmer (thin dashed dark red curve versus dashed green curve), by comparison to the no-pathogen case where the two phenotypes have identical fitness (the overlapping dashed blue curve and thick dashed red curve). However, in isolation, populations of farmers with increased mortality (green solid curve) fare better than populations of farmers with no mortality cost associated to farming (blue solid curve). This is because individual mortality results in reduced predation pressure on the bacteria which can grow better and ultimately support a larger population of worms. Thus, increased mortality (e.g. due to feeding on pathogenic bacteria) is not something to be avoided if the worms are most likely to interact with their own kind. Left panel = plate size $R = 2.5cm$; right panel = plate size $R = 7.5cm$. Overall, larger plates allow for more farming, which leads to farmers in isolation (blue and green solid curves) reaching larger abundances than the exploiting non-farmers (red curves). Parameters are once again taken from Table S1.

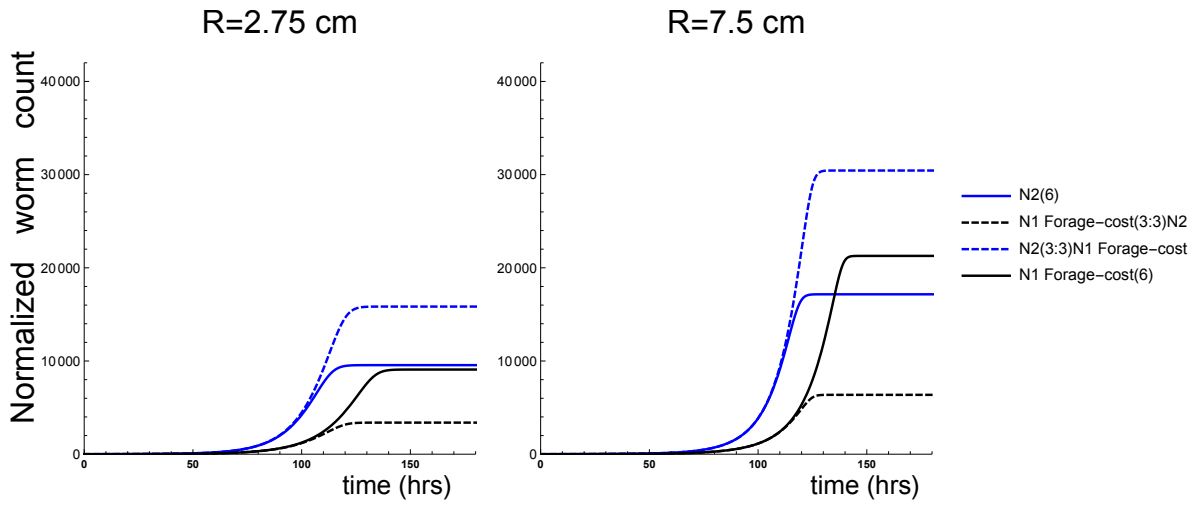

Figure S12: Worm counts normalized by initial worm numbers of each phenotype. Phenotype $N1$ is a more efficient forager than $N2$ ($\sigma^{(1)} > \sigma^{(2)}$) but pays a metabolic cost reflected by a lower egg-laying rate ($\epsilon_1^{(2)} > \epsilon_1^{(1)}$) due to the energetic demands of its foraging. We show two different plate sizes. Blue curves = $N2$; black curves = $N1$. The better forager who simultaneously incurs a cost fares worse (dashed black) than the poorer forager (dashed blue). In isolation however, the better forager who plays a cost (solid black) can fare better due to the reduced pressure it places on the bacterial population. These effects are more likely to be seen as plate size increases because only big enough plates show significant differences between the two foraging strategies – on small plates both $N1$ and $N2$ are similarly good foragers.

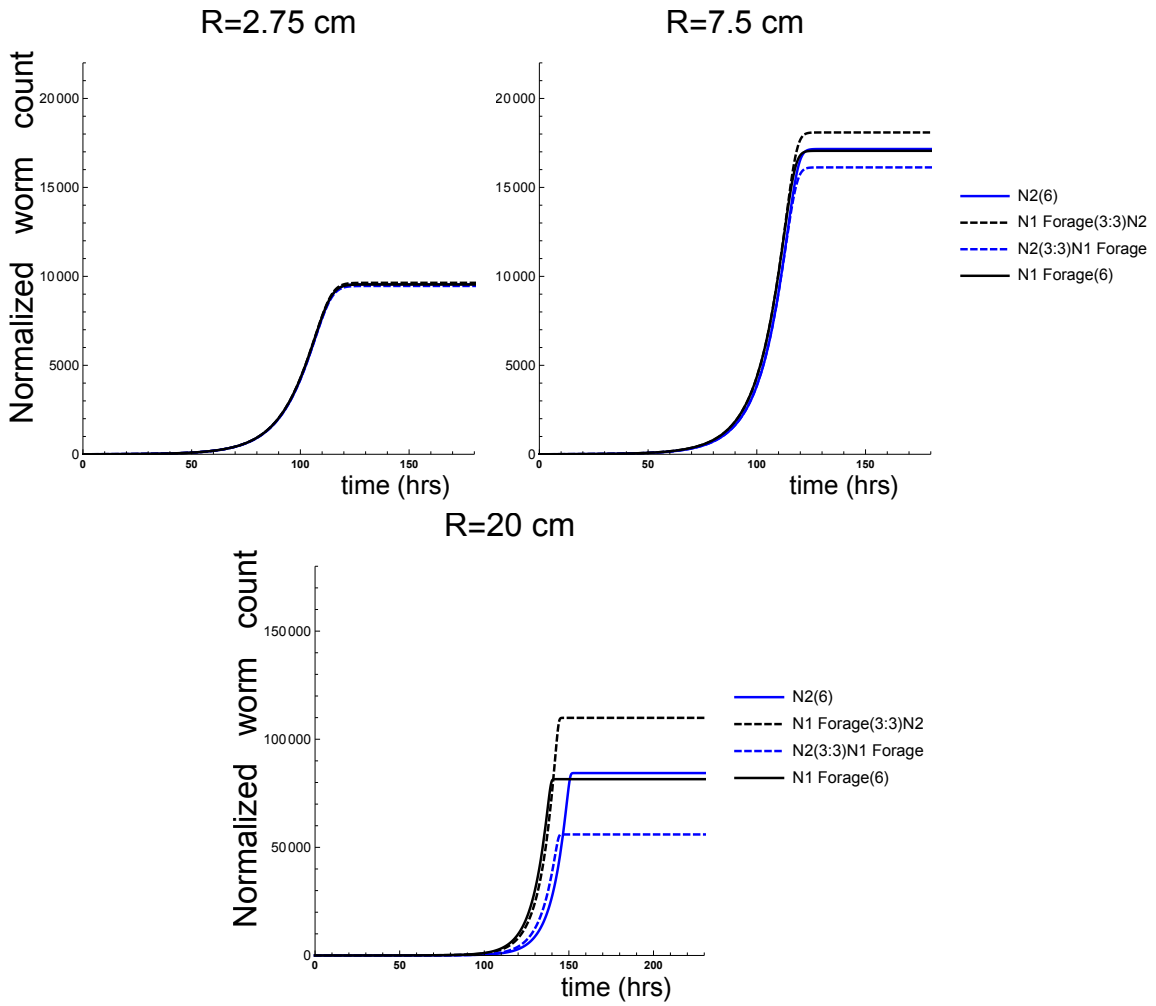

Figure S13: Worm counts normalized by initial worm numbers of each phenotype. Phenotype $N1$ is a more efficient forager than $N2$ ($\sigma^{(1)} > \sigma^{(2)}$) and pays no metabolic cost for this behavior ($\epsilon_1^{(2)} = \epsilon_1^{(1)}$). We show three different plate sizes. As in Figure S12, blue curves = $N2$; black curves = $N1$. The better forager out-competes the other phenotype (dashed black compared to dashed blue), however the effect is exacerbated on larger plate sizes. Once again, the form of the encounter rate, Eq. (S.9), is such that for small plates both $N1$ and $N2$ are similarly good foragers. In isolation, the better foraging $N1$ worm reaches slightly lower numbers than the $N2$ worm, in a manner reminiscent of Figure S12; it forages too well initially, placing an increased pressure on the bacteria, ultimately resulting in a smaller population. However the effect is very minor for small plate sizes.

Tables

Param.	Units	Value	Justification
g_A g_ρ K_ρ	min^{-1} min^{-1} cells/cm^2	1.13×10^{-4} 1.07×10^{-3} 4.58×10^{8}	These parameters are derived from fitting Eqs. (S1) and (S2) to the data in Figure S2. In the fitting it is assumed that florescence intensity is directly proportional to the number of cells. The mapping from cell number to florescence intensity is determined from the initial number of cells on the plate, $N_B(0)$ (see below).
K_A	cm^2	$[\pi 2^2, \pi 25^2]$	The bacteria area carrying capacity is equal to the area of the plate.
a	cells/min	70	Worms have been identified as eating around 70 cells per minute [1].
$\epsilon_1/\epsilon_1^{(2)}$	min^{-1}	3.08×10^{-2}	Experimental results indicated that N2 and srf-3 lay a joint average of 44 embryos per day for 4 days (see Figure S3b).
τ_{hatch}	min	540	Eggs take approximately 9 hours to hatch [2].
ϵ_2	min^{-1}	2.98×10^{-4}	Yields 56 hour mature time. This is the approximate mature time given in literature [2].
d	min^{-1}	1.74×10^{-4}	Worms reproduce for approximately 4 days (see Figure S3b).
δ	$\text{cells}^{-1}\,\text{cm}^2\,\text{min}^{-1}$	8×10^{-13}	Illustrative parameter for exploring model behavior and potential experimental outcomes. Used in Figure S11.
$\epsilon_1^{(1)}$	min^{-1}	$(\epsilon_1^{(2)}/1.5) = 2.05 \times 10^{-2}$	Illustrative parameter for exploring model behavior and potential experimental outcomes. Used in Figures S12-S13.
$\sigma^{(1)}$	cm^2	$1.5 \times \sigma^{(2)} = 1400$	Illustrative parameter for exploring model behavior and potential experimental outcomes. Used in Figures S12-S13.
$N_B(0)$	cells	10^8	Initial number of cells plated in experiments .
$A_B(0)$	cm^2	$\pi 0.5^2$	Initial patch size in experiment.
$\rho(0)$	cells/cm^2	1.27×10^{8}	Initial bacterial concentration.
c	cells^{-1}	2.5×10^{-9}	Parameter chosen to illustrate good visual qualitative fit with data in Figure 3 (see Figure S7). Used in Figures S7-S13.
$\sigma/\sigma^{(2)}$	cm^2	1000	Parameter chosen to illustrate good visual qualitative fit with data in Figure 3 (see Figure S7). Used in Figures S7-S13.
s	$\text{min}^{-1}\text{cm}^{-2}$	7×10^{-9}	Parameter chosen to illustrate good visual qualitative fit with data in Figure 3 (see Figure S7). Used in Figures S7-S13.

Table S1: Parameters used throughout document. Free parameters are highlighted in red.

References

[1] R. L. Gomez-Amaro, E. R. Valentine, M. Carretero, S. E. LeBoeuf, S. Rangaraju, C. D. Broaddus, G. M. Solis, J. R. Williamson, and M. Petrascheck, "Measuring food intake and nutrient absorption in caenorhabditis elegans," 200(2):443-54. *Genetics*, 2015.

[2] Z. F. Altun, and D. H. Hall, "Introduction. In WormAtlas", 2009. doi:10.3908/wormatlas.1.1